RESEARCH ARTICLE

Fabrication, characterization and optimization of berberine-loaded PLA nanoparticles using coaxial electrospray for sustained drug release

Reza Ghaffarzadegan[1,2] · Sepideh Khoee[3] · Shamsali Rezazadeh[2]

Abstract

Background Berberine (BBR) broadly found in medicinal plants has a major application in pharmacological therapy as an anticancer drug. Clinical applications of this promising natural drug are limited due to its poor water solubility and low bioavailability.

Objective In this study, for the first time, we synthesized core-shell BBR-loaded PLA nanoparticles (NPBs) by using coaxial electrospray (CES) to solve the poor bioavailability of BBR.

Methods Three-factor (feeding rate, polymeric solution concentration and applied voltage), three-level, Box-Behnken design was used for optimization of the size and particle size distribution of the prepared NPBs.

Results Based on the results of response surface methodology, the NPBs with the mean size of 265 nm and particle size distribution of 43 nm were synthesized. A TEM image was used to well illustrate the core-shell structure of the NPBs. Encapsulation efficiency and BBR loading capacity for the optimized NPBs were determined at about 81% and 7.5%, respectively. Release of NPBs was examined at pH 7.4 and 5.8. NPBs had a slower release profile than free BBR in both pH values, and the rate of BBR release was more and faster in acidic pH than in physiological one. Effects of the NPBs on the drug release were confirmed by data fitting with six kinetic models. NPBs showed an increased cytotoxic efficacy against HCT116 cells (IC$_{50}$ = 56 μM), while NIH3T3 cells, non-neoplastic fibroblast cells, (IC$_{50}$ > 150 μM) were less affected by NPBs. Flow cytometry demonstrated that the cellular uptake of NPBs were higher than BBR at different concentrations.

Conclusions A new approach was developed in this study to prepare NPBs using the CES process for improving the efficiency and controlled BBR release. It is concluded that nano-scaled NPBs prepared by CES can improve toxicity and chemotherapeutic properties of BBR against cancerous cells. We believe that these NPBs can exhibit further potential in cancer drug delivery systems.

Keywords Berberine · Coaxialelectrospray · Optimization · particle size · Release · Cytotoxic efficacy

✉ Sepideh Khoee
khoee@khayam.ut.ac.ir

1 School of Chemistry, Alborz Campus, University of Tehran, Tehran, Iran

2 Medicinal Plants Research Center, Institute of Medicinal Plants, ACECR, Karaj, Iran

3 Polymer Laboratory, School of Chemistry, College of Science, University of Tehran, PO Box 14155 6455, Tehran, Iran

Introduction

In the current century, the field of drug discovery has been extensively linked to medicinal plants throughout the world [1]. Berberine (BBR), an herbal alkaloid drug, is obtained from the roots and stem bark of *berberis* species [2]. BBR has different pharmacological applications such as antiviral, antibacterial, antifungal, antimalarial, antisecretory, antileishmanial, antidiabetic, and anticancer applications and also has anti-Alzheimer's disease effect [3–7]. BBR is one of the well-known anticancer drugs for the treatment of hepatoma, breast cancer, bladder cancer, and colon cancer [8]. However, clinical applications of this promising natural drug

🖄 Springer

are limited due to its low water solubility and low bioavailability [9–11]. Therefore, to overcome these problems, researchers have focused on designing nano-dimensional particles to enhance the bioavailability and solubility of BBR delivery [12, 13]. Two methods developed to fabricate BBR NPs with evaporative precipitation of nanosuspension (EPN) and anti-solvent precipitation to improve the bioavailability and solubility of BBR molecules [14].

Folic acid-modified chitosan nanoparticles loaded with BBR (BH/FA-CTS NPs) were synthesized for nasopharyngeal carcinoma therapy using the ionic cross-linking method to overcome the weaknesses of BBR as a poorly soluble and bioavailable drug [15].

Nowadays, numerous approaches have been introduced to improve the bioavailability and solubility of hydrophobic drugs, such as microemulsion, micelle, and microparticles [16–21]. Polymeric biodegradable micro/nanoparticles are currently being widely explored for the therapeutic development of novel drug delivery systems, because of their high dissolution rates that improve drug stability, bioavailability, and controlled release behavior [22–24]. Recently, several types of polymers such as polycaprolactone, polyethylene glycol, poly (lactic-co-glycolic) acid, polyvinyl alcohol, and chitosan have been extensively used in biomedical applications due to their excellent biodegradability in the body [25–30]. Specifically, polylactic acid (PLA) has been extensively used as a biomaterial system such as drug delivery, artificial skin, wound dressing, and bone and tissue engineering due to its superior biodegradability, biocompatibility, non-toxic, and high mechanical properties [31–36]. The electrospray (ES) process has shown significant potential for preparing monodisperse NPs from a group of various precursors to generate polymeric drug delivery systems so that drugs can be encapsulated with low solubility in water [37]. Nano-encapsulation can improve the chemical stability of core-loaded drugs and help controlled release rates in the in-vivo environment [38]. This technique is one of the most commonly used processes to prepare a liquid droplet using a strong electric field that helps to prepare different nanostructures by overcoming the electrostatic repulsion of a polymeric droplet to the surface tension energy of a polymer solution [39–41].

In comparison with conventional electrospray, coaxial electrospray is an electrohydrodynamic process for the preparation of multilayer nano- and microparticles using coaxial electrified jets. This technic has great and different advantages such as effective protection of bioactivity, high encapsulation efficiency and uniform size distribution over the other fabrication processes like emulsification, soft lithography, polymeric micelles, spray drying and microchannel extrusion [42]. Recently, coaxial electrospray (CES) has been applied to synthesize core-shell nanoparticles (NPs) [43]. In this system, uniform electric potential connected to two capillary needles. Hydrophobic drugs and organic solvents flow in the

interior capillary needle, and a polymeric solution flows in the exterior capillary needle.

Design of experiment (DOE) is a mathematical and statistical approach for modeling and optimization of synthesized nanoparticles [44].

The purpose of this study was to prepare and optimize nano-sized core-shell NPs based on berberine-loaded PLA particles using the CES technique to improve the bioavailability of BBR. To the best of our knowledge, this is the first study on using CES for the preparation and optimization of NPBs to enhance drug loading (DL) efficacy and controlled/sustained release behavior.
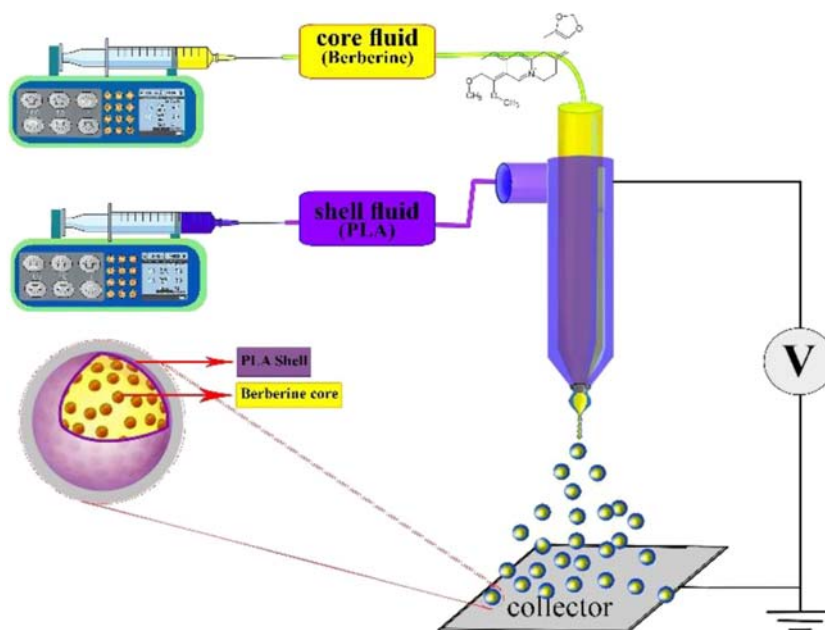
Materials and methods

Materials

PLA (averaged Mw by GPC = 300 kDa,) was kindly gifted by Isfahan university. BBR chloride, dimethylformamide (DMF), ethanol, and chloroform (analytical grade) were purchased from Sigma-Aldrich. Phosphate buffer saline (PBS) was purchased from Bio Basic Inc. HCT116 (human colorectal carcinoma cells) and NIH3T3 (Swiss mouse embryo fibroblast) were prepared from the Pasteur Institute of Iran (Tehran, Iran). The Roswell Park Memorial Institute medium (RPMI) 1640, Dulbecco's modified Eagle's medium (DMEM), and fetal bovine serum (FBS) were purchased from Biosera (UK). Pen-strep and trypsin-EDTA were purchased from Gibco (UK). MTT (3-[4, 5-dimethylthiazol-2-yl] 2, 5-diphenyl tetrazolium bromide) was purchased from Sigma (Germany). All other materials and reagents applied in this work were of analytical grade unless otherwise noted.

The experimental setup

The schematic pattern of the CES apparatus used for the preparation of BBR-loaded PLA NPs is illustrated in Fig. 1.

In this work, the CES process included two syringe pumps (JMS SP-500, Japan), a coaxial needle, and high voltage DC power supplies. The coaxial needle consisted of an inner needle with 18-gauge and an outer needle with 22-gauge. Briefly, different amounts of PLA were dissolved in a chloroform/DMF mixture with a ratio of 2:1 to prepare a 0.1–0.5% (w/w) polymeric solution and berberine hydrochloride was dissolved in an ethanol/DMF mixture with the ratio of 2:1. The polymeric solution was stirred (100 rpm) for 24 h at room temperature to form a homogeneous solution. Then, BBR and PLA solutions were poured into two 5 mL plastic syringes with the polymer/drug ratio of 10:1% (w/w), as core and shell layers, respectively. Afterward, two pumps were applied to deliver the PLA and BBR solutions through a coaxial system. The distance between the tip of the needle and the collector

was fixed on 18 cm. The drug solution was sprayed at the flow rate of 0.25 mL/h and the polymeric solution was electrosprayed at the flow rate of 1–2 mL/h. The applied voltage was tuned on 16–20 kV and the polymer concentration was 0.1–0.5%. Finally, the NPs were collected on an aluminum foil surface after 1 h. Table 1 shows the details of the experimental parameters.

Characterization

The morphology, particle size, and size distribution of the NPBs were measured using Field emission scanning electron microscopy (FE-SEM, Nova NanoSEM 450). The particle size of the NPBs was measured for pre-tests using an optical microscope (Nikon ECLIPSE E100, USA). The average mean size and particle size distribution (PSD) were calculated by the Image J software. Transmission electron microscopy (TEM, Philips 208S) was utilized to evaluate the core-shell structure of NPBs. Fourier transform infrared (FT-IR) (BRUKER, Germany) was applied to characterize the NPBs. Moreover,

the BBR release behavior of the NPBs was measured by a UV-Vis spectrophotometer (X-ma 2000). Calorimetric measurements were studied using TA-2 (Pishtaz engineering Co., Iran). The analysis was performed in the range of 25 to 250 °C with a heating rate of 5 °C/min in an air atmosphere.

Experimental design

According to the pre-tests, the concentration, voltage, and flow rate of the polymeric solution were selected as independent variables. These variables were defined at three levels: low (−1), basal (0) and high (+1), as given in Table 1. The Box-Behnken model obtained by the Design-Expert Software (Version 11 State-Ease, USA) suggested 15 experiments, including 12 factorial points and 3 replicates of the central point, to estimate the pure error and sum of squares **(Table S1)**. A mathematical relationship was obtained between the independent variables (X_i,...) and responses (particle size and size distribution) by a second-order polynomial function model as below:

$$Y = \alpha_0 + \alpha_1 X_1 + \alpha_2 X_2 + \alpha_3 X_3 + \alpha_{11} X_1^2 + \alpha_{22} X_2^2$$
$$+ \alpha_{33} X_3^2 + \alpha_{12} X_1 X_2 + \alpha_{13} X_1 X_3 + \alpha_{23} X_2 X_3 \quad (1)$$

Where, X_1, X_2, and X_3 are independent variables; Y is the predicted response; α_0 is the intercept; α_1, α_2, and α_3 are the linear coefficients; α_{11}, α_{22}, and α_{33} are the squared coefficients, and α_{12}, α_{13}, and α_{23} are the interaction coefficients of the equation. In the present work, contour plots as 3D surface plots were applied to show the relationship and interaction between the independent variables and the dependent responses.

Table 1 Parameters used in design of experiment

Independent variable	Symbol	Levels		
		−1	0	+1
Concentration (w/w %)	X_1	0.1	0.3	0.5
Flow rate (mL/h)	X_2	1	1.5	2
Voltage (kV)	X_3	16	18	20
Dependent variables	Constrains			
Y_1 = particle size	Minimize			
Y_2 = particle size distribution	Minimize			

Calculation of the encapsulation efficiency (EE) and drug loading (DL) of the NPBs

EE and DL of BBR in NPBs were determined as follows: Initially, 30 mg of NPBs were added into 30 mL of ethanol, the solution was shaken for 1 h and washed for several times until the yellow color of BBR disappeared. The content of BBR in the NPBs was characterized by UV-Vis spectroscopy at the wavelength of 348 nm. Equations (2) and (3) were used to calculate DL and EE, respectively.

$$DL\ (\%) = B_t - B_s / B_N \times 100 \qquad (2)$$

$$EE\ (\%) = B_{t-}B_s / B_t \times 100 \qquad (3)$$

Where B_t, B_s, and B_N are the initial weight of BBR, the weight of the detected BBR in the solution, and the weight of the NPBs, respectively.

In vitro drug release from the PLA NPs

To determine the drug release properties of the NPBs, 30 mg of particles were placed in each dialysis bag (cut-off 12 kDa) and then two dialysis bags were immersed in vessels including 50 mL PBS with pHs 5.8 or 7.4. Afterward, the dispersed NPs in PBS was put in an incubator to supply a suitable ambiance in terms of darkness and temperature with the velocity of 100 rpm at 37 °C. At determined intervals, 2 mL of the re-leased solution was taken to investigate the release amount of BBR and then the same amount of the fresh PBS solution was replaced immediately to maintain the volume constant. The release solution was analyzed by a UV-Vis spectrophotometer at 348 nm. The cumulative drug release percentage of BBR was calculated using Eqs. 4 and 5 [45].

$$B_{rmod} = B_r + (V_s / V_t) \sum Br \qquad (4)$$

$$Cumulative\ release\ rate\ (\%) = B_{rmod} / B_{total} \times 100\% \qquad (5)$$

Where B_r and $B_{r\ mod}$ are the evident weight and modified weight at the time of t, V_S is the volume of the taken sample, V_t is the total volume of the release medium, $\sum B_r$ is the sum-mation of B_r, and B_{total} is the total weight of BBR entrapped inside the particles.

Colloidal stability studies

Colloidal stability analyses were conducted at 25 °C, during three weak (once a week) using a DLS instrument. Samples were prepared in deionized water and their concentrations were adjusted to be 50 μg/mL. **Eq.6** was used to determine the colloidal stability of the particles.

Colloidal Stability t_n

$$= \frac{Nanocarrier\ size\ (t_n)}{Initial\ size\ of\ the\ nano\ carriers\ (t_0)} \qquad (6)$$

Where the colloidal stability of the particles in each week (t_n) equals to the nanocarrier size in each week (t_n) to the initial size of the nanocarrier at the beginning of the test (t_0).

Evaluation of in vitro cytotoxicity

The mitochondrial tetrazolium test was conducted to as-sess the viability of NIH3T3 and HCT116 against various concentrations of the sample. The above-mentioned cell lines were maintained as exponentially growing cultures in either the DMEM or RPMI 1640 cell culture medium supplemented with 10–15% FBS and antibiotics, under culture conditions. The nano-formulation was used at con-centrations ranging between 0.586–150 μg/mL doubling dilutions, and the cells were incubated for 24, 48, and 72 h. After each interval, the cells were treated by the MTT solution (5 mg/mL) and the absorbance was mea-sured at 570 nm and referenced at 630 nm. Each experi-ment was performed in four replications and cells with no treatment were considered as control. The concentration required for 50% inhibition of cell viability (IC50) was determined by nonlinear regression analysis and expressed in the mean ± standard error of the mean (SEM).

Statistical analysis

Statistical differences between the treatment and control groups were examined by one-way analysis of variance followed by Turkey's tests (Stats-Direct version 3.1.18). Differences were considered statistically significant at $P < 0.05$.

Cellular uptake of NPBs and BBR by flow cytometry

The HCT-116 cells were cultured in 12-well plates at an appropriate density for 24 h. In the following day, a fresh medium containing BBR (at 1/2 concentration of its $IC_{50} = 70.773$ μg/mL) and NPBs (at 1/2 and 1/5 concen-trations of its $IC_{50} = 56.825$ μg/mL) were added to the individual dishes (in separate wells) and incubated for additional 24 h. Untreated cells were considered as con-trol. Consequently, cells were tripsinized, collected and re-suspended in PBS for analysis. The fluorescence inten-sity of cells was quantitated using FACS flow cytometer at 488 nm excitation and 585/40 band-pass (FL2) filter. Data were analyzed using FlowJo v10 software. FSC vs. SSC gating was used to remove cell debris, and the

fluorescent histogram parameters were determined from this gated scatter region [46].

Results

Different parameters and their importance

Solution parameters, like types of polymer and solvents, and the ratio of different solvents are more important than ambient variables. DMF and chloroform were chosen as solvents at the ratios of 1:1, 1:2 and 1:3 in order to obtain suitable miscibility and a favorable amount of conductivity to reach a stable Taylor cone (Fig. 2a-c). After carrying out the pre-tests, the ratio of 2:1 (Chloroform:DMF) was chosen as the best ratio. Figure 2b shows the suitable dispersion and morphological characteristics at the ratio of 2:1 compared to the ratios of 1:1 and 3:1 shown in Fig. 2a and c, respectively. In addition, the distance between the nozzle and the collector was investigated as another important process variable. Distances of 16,
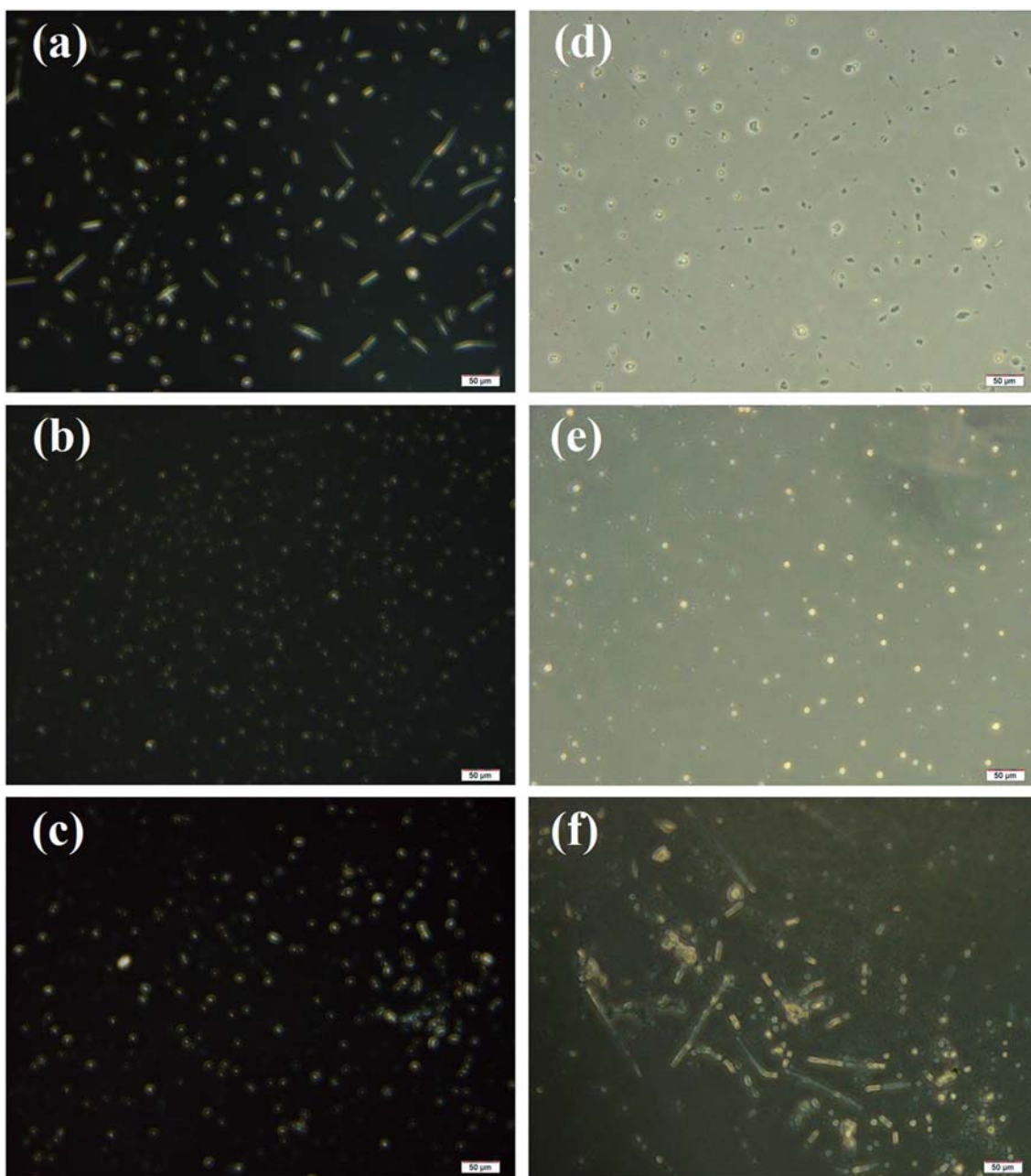
Fig. 2 Optical images of particles using different solvents: 1:1 (a), 2:1 (b), 3:1 (c) and different distances: 16 (d), 18 (e) and 20 (f) cm

18 and 20 cm were considered as desired values (Fig. 2d-f). By carrying out the pre-tests, the 18 cm distance was diagnosed as the best distance (Fig. 2e).

Response surface analysis and model fitting for size and size distribution

The SEM analysis was used for investigating the size and size distribution of the synthesized NPBs by the CES process. About 50 particles were chosen randomly and mean size and PSD from each image were determined. The mean size and size distribution of the NPBs were obtained, ranging between 266 and 457 nm and 43–90 nm, respectively (**Table** S1). The analysis of variance (ANOVA) was employed by calculating the F-value to find the best model fitting well with our experimental data.

The results of ANOVA for particle size and size distribution are shown in **Table** S2 and Table 2, respectively. In both responses, the models were significant and "lack of fit" was "insignificant".

The quadratic second-order equation fitting with the experimental data for size had the following expression:

$$Y_1 = 2785.17 + 143.12X_1 - 300.25X_2 - 245.31X_3$$
$$+ 305X_1X_2 - 47.5X_1X_3 + 655.2X_1{}^2 + 81.83X_2{}^2$$
$$+ 6.61X_3{}^2 \tag{7}$$

The quadratic second equation fitting with the experimental data for PSD had the following expression:

$$Y_2 = 611.46 + 185X_1 - 42.5X_2 - 59.5X_3$$
$$+ 55X_1X_2 - 19.37X_1X_3 + 190.62X_1{}^2 + 1.65X_3{}^2 \tag{8}$$

Where Y_1 and Y_2 demonstrate the size and PSD and X_1, X_2, and X_3 are the concentration, the flow rate of the polymer and the voltage, respectively.

The R^2 values of the model for size and PSD were obtained 0.9908 and 0.9815, respectively. Moreover, the adjusted R^2 values were obtained 0.9742 and 0.9481, respectively. The obtained data of the adjusted R^2 values suggested that only 2.58% and 5.19% of the total variation in the model were not explained by the variable factors. The p values of the models for size and PSD were 0.0001 and 0.0008, respectively. Results revealed that both models were highly significant. Figures 3 and 4 demonstrate the effect of the independent variables on size and size distribution with the graphical plots obtained from the software.

Figure 3a shows that there is a direct relationship between flow rate and concentration with particle size. So that by increasing the solution flow rate or concentration, the particle size of the NPBs increased.

Figure 3b illustrates the effect of voltage on the final particle size of the NPBs. In fact, by increasing the voltage from 16 to 20 kV, a decrease in particle size was observable.

X_i = independent parameters, Df = degrees of freedom, Cor Total = Total (corrected).

To reach the optimum values for PSD, the CES process should be performed in stable cone-jet mode [47]. Figure 4a reveals that by enhancing the concentration of the polymeric solution, PSD will increase.

According to Fig. 4a, in the concentration range around 0.2 to 0.4 (%) and the flow rate from 1 to 1.2 (mL/h), the lowest and consequently the optimum amount of PSD was observed.

Figure 4b illustrates the indirect relationship between the applied voltage and PSD. As shown, an increase in voltage decreased PSD values. By the plot, the lower values of PSD were obtained in the 18–20 kV voltage domain.

Table 2 ANOVA results for PSD

| Source	Sum of Square	df	Mean Square	F-value	p value	
Model	2050.85	9	227.87	29.40	0.0008	**significant**
X_1	351.13	1	351.13	45.31	0.0011	
X_2	420.50	1	420.50	54.26	0.0007	
X_3	561.12	1	561.12	72.40	0.0004	
X_1X_2	121	1	121	15.61	0.0108	
X_1X_3	240.25	1	240.25	31	0.0026	
X_2X_3	4	1	4	0.5161	0.5047	
$X_1{}^2$	214.67	1	214.67	27.70	0.0033	
$X_2{}^2$	12.98	1	12.98	1.67	0.2521	
$X_3{}^2$	162.06	1	162.06	20.91	0.0060	
Residual	38.75	5	7.75			
Lack of Fit	36.75	3	12.25	12.25	0.0764	**not significant**
Pure Error	2	2	1			
Cor Total	2089.60	14				

Fig. 3 The 3D response surface plots for analysis of a) flow rate and PLA concentration, b) applied voltage and PLA concentration on particle size
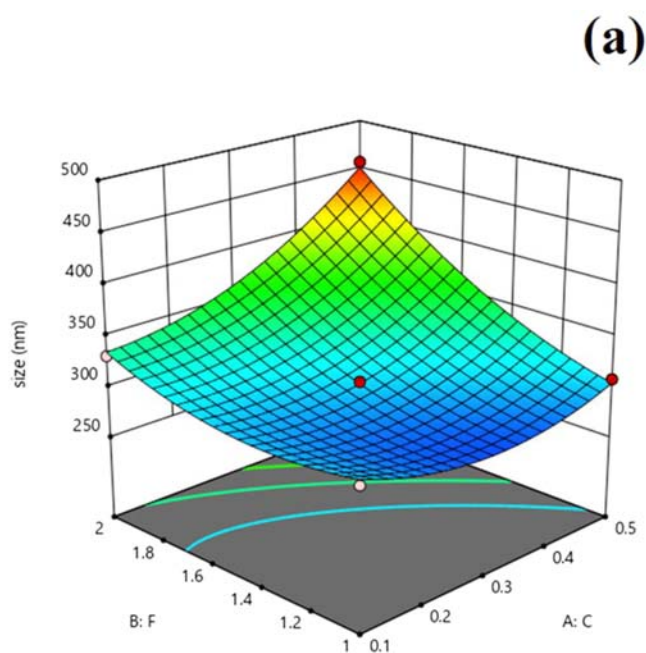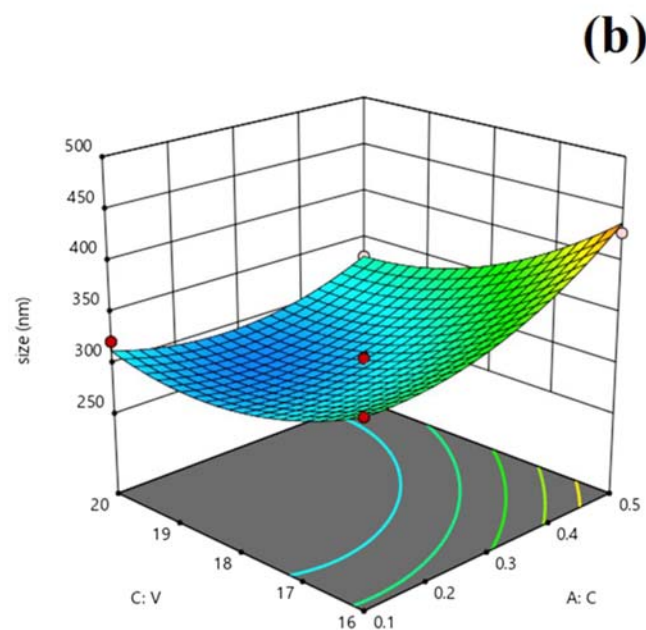
Determination of optimal conditions for the preparation of the NPBs.

Solving the quadratic equations led to determining the optimum values of the polymer concentration (0.35%w/v), feeding rate (1.03 mL/h), and applied voltage (19.47 V). The lowest value was predicted by the software for size in 265 nm and PSD in 41 nm. These obtained results are the optimum values in this study. To evaluate the suggested model, the experiments were repeated three times in the optimum condition. The output results obtained from the SEM images presented 270 nm for mean particle size and 44 nm for PSD (Fig. 5a).

Besides, standard deviation (SD) equal to 4.6 and 5.2% was measured for these two parameters data analysis, respectively.

TEM analysis was applied to characterize the core-shell morphology of the NPBs, which was synthesized under the optimum condition. Figure 5b demonstrates an obvious difference between the core and the shell, which confirmed that our coaxial needle worked well.

The FT-IR of PLA, BBR, and optimized NPBs are shown in Fig. 6. In the PLA spectrum, the peaks at 1747 and 1081 cm^{-1} can be ascribed to the stretching vibration of C=O and C–O bands, respectively. Moreover, asymmetrical
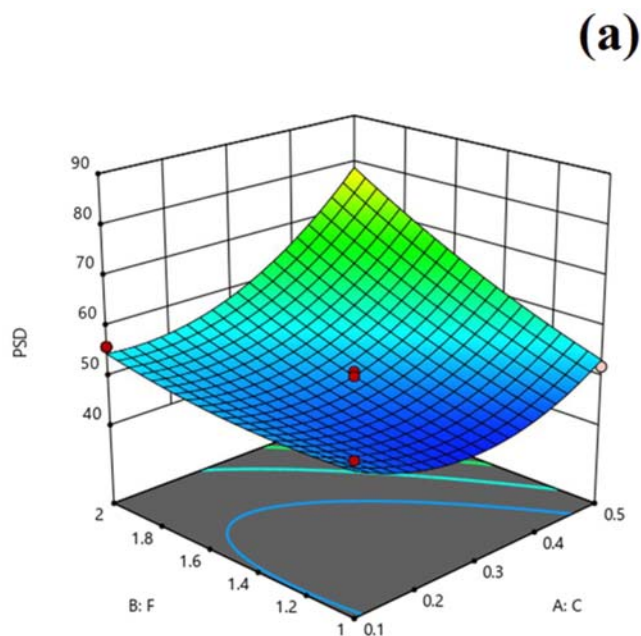
Fig. 4 The 3D response surface plots for analysis of a) flow rate versus concentration and b) applied voltage versus concentration on PSD
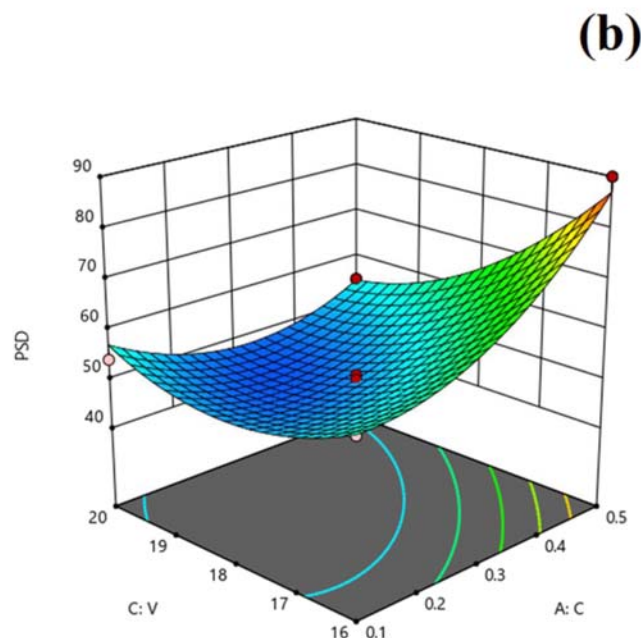
vibrations of -CH3 bands at 1451 and 1362 cm^{-1} are distinguishable (Fig. 6a). Two weakly sharp peaks at 2952 and 2845 cm^{-1} are related to the C-H stretching bond in aliphatic -CH$_2$ and CH$_3$ groups of berberine. Moreover, the peak at 1603 cm^{-1} can be attributed to the iminium (C=N$^+$) bond (Fig. 6b). The FT-IR spectrum of the NPBs exhibited both peaks of PLA and some weak peaks of BBR, which confirmed the preparation of the drug-loaded NPs. The peaks at 1751 and 1076 cm^{-1} can be related to the stretching vibration of C=O and C–O bonds of PLA. A medium peak at 1279 cm^{-1} is related to the C-N stretching bond in berberine (Fig. 6c).

Figure 7 illustrates the thermograms of PLA, berberine, physical mixture of berberine/PLA along with berberine-loaded nanoparticles (NPBs). Pure BBR showed a sharp endothermal peak at around 195 °C, which was ascribed to the melting point of the crystalline structure of the drug. Moreover, the broad endothermal peak of dehydration of BBR could be observed between 95 and 130 °C. The DSC curve of PLA exhibited a sharp endothermal peak at around 200 °C, which was related to the melting point of the polymer. In the physically blended BBR and PLA sample, all the characteristic peaks of BBR and PLA
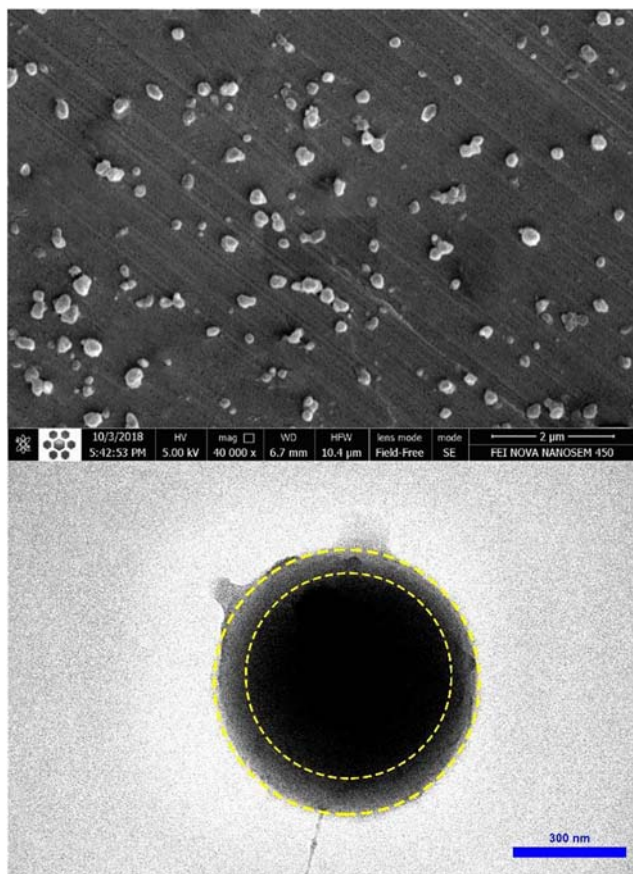
Fig. 5 SEM (a) and TEM (b) micrographs of NPBs

Fig. 7 DSC of Berberine, PLA, Physically blended berberine/PLA and NPBs

are present but all are shifted to higher temperatures by nearly 20 °C. This change in the positions of peaks may represent the formation of physical interaction between drug and polymer without destroying the crystallinity of starting materials. While the disappearance of drug and polymer peaks in NPB demonstrates a high degree of crystallinity loss that can be related to the decreasing in
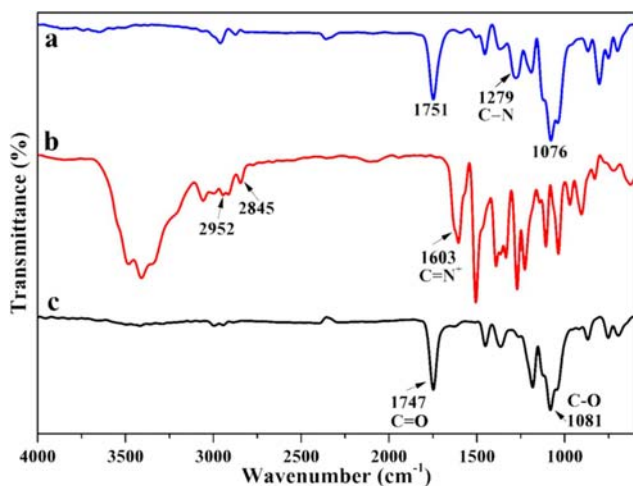
the crystallinity of the pure BBR and also PLA chains by penetrating the BBR molecules into and between the chains of PLA.

Encapsulation efficiency (EE) and drug loading (DL)

The EE and DL of the NPBs synthesized in the optimum conditions were calculated around 81% and 7.5%, respectively. Encapsulation efficiency greatly depends on the interactions between the PLA and BBR. The most common form of berberine for loading and release is the salt form of drug, *i.e* berberine hydrochloride. Entrapment of hydrophilic berberine inner the hydrophobic shell could reduce the encapsulation efficiency [48] to enhance the berberine hydrochloride affinity with hydrophobic polymer, complexing the drug with phospholipid was applied [9]. Here, we used a mixture of solvents to increase the solubility parameter of drug in polymer, accordingly, NPBs shows significant encapsulation efficiency and drug loading.

In vitro drug release

The drug release profile of the NPBs prepared using the CES process was evaluated and compared with free BBR in two pHs of 7.4 and 5.8, as shown in Fig. 8, the BBR release rate from the NPBs was significantly slower than the free BBR. In

Fig. 6 FT-IR spectra of a) PLA, b) Berberine, and c) NPBs

Fig. 8 In vitro drug release profiles of BBR and NPBs at two pHs 7.4 and 5.8
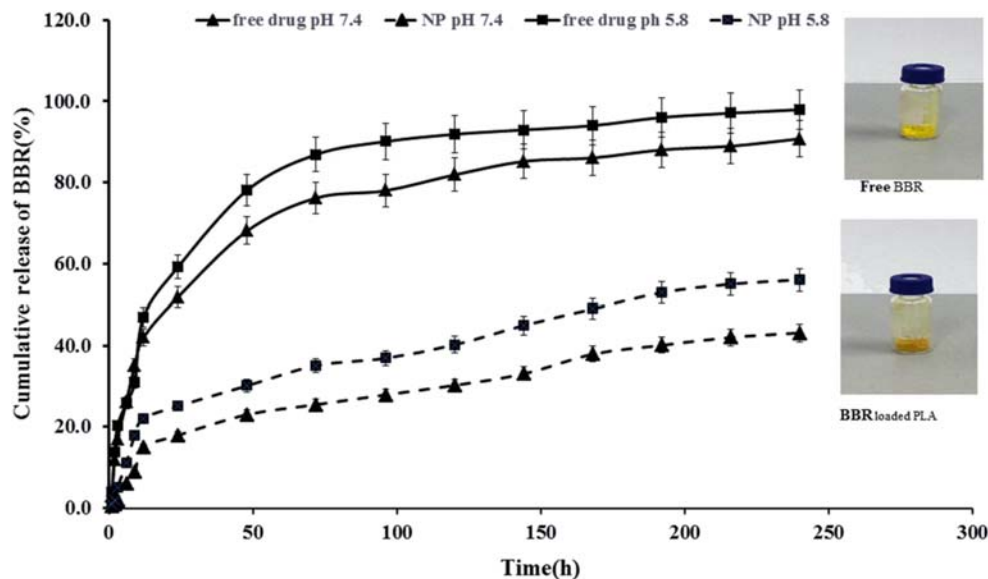
acidic pH, the amount of released BBR from the NPBs was around 57% over 240 h. However, in physiological pH, the amount of the BBR released from the NPBs was 43% over 240 h. The burst release was observed in the first 12 h and then, a sustained controlled release occurred. In order to obtain more information in this regard, we performed kinetic modeling.

We used modeling to study the release profile behavior of BBR and NPBs in two different pHs. Six most applicable models such as Zero-order, First-order, and power low, Higuchi, Hickson-Crowell, and Korsmeyer-Peppas were used. The statistical parameter of the coefficient of determination (R^2) was used for fitness criteria, which yielded great information about the quality of fitting. The root means squared error (RMSE) was commonly used in the non-linear regression. Based on the R^2 and RMSE indices, the power low model was the finest fitted model for pure BBR in both pHs of 7.4 and 5.8 (**Table** S3). Moreover, at a pH of 7.4, by loading BBR into PLA, the burst release section of the drug release followed the Korsmeyer-Peppasmodeling. The sustained section of the release profile followed zero-order modeling. At a pH of 5.8, both sections of the burst release and sustained release followed the zero-order modeling and almost the release of the drug was under control.

DLS analysis was utilized for three successive weeks to determine the size of nanoparticles and consequently, specify the colloidal stability of nanocarriers using **Eq. 6**. The obtained results have shown that the colloidal stability of the above-mentioned nanocarriers was around 1.02–1.19 after three weeks of investigation (Fig. 9). Hence, according to the reported acceptable optimum amount of diameter change in the literature (1–1.5) [49], the synthesized nanocarriers have shown appropriate colloidal stability.

The NPBs cytotoxicity

We found that the number of HCT116 cells was reduced in the presence of the NPBs in the culture medium (Fig. 10). The inhibitory effect on tumor cell proliferation was dose-dependent and the sample appeared to be a potent inhibitor of tumor cell proliferation, particularly at 72 h. NPBs demonstrated cytotoxic effects on HCT116 and NIH3T3 cells with the IC_{50} values of 56.82 and > 150 μg/mL, respectively. Non-neoplastic NIH3T3 cells were much less affected by the sample in comparison with the cancerous cells.

The IC_{50} values presented in **Table S4** showed that the sample was different from the control group ($P < 0.05$) and demonstrated cytotoxic activity on the experimental cell lines. Interestingly, the NPBs showed strong inhibitory activity against HCT116 cells after 72 h, while NIH3T3 fibroblast cells (as non-neoplastic cells) were less affected by the sample
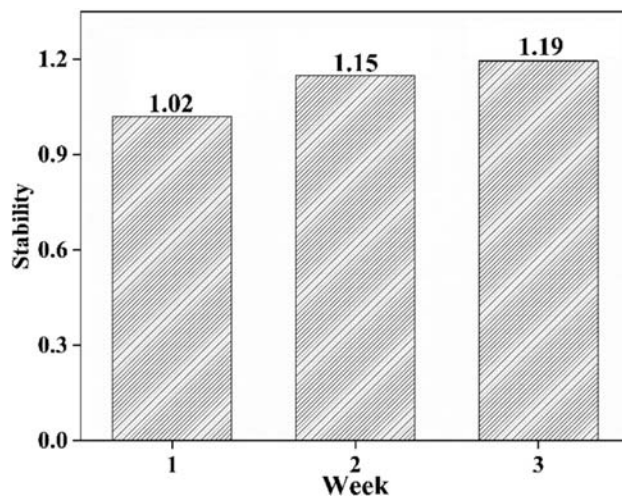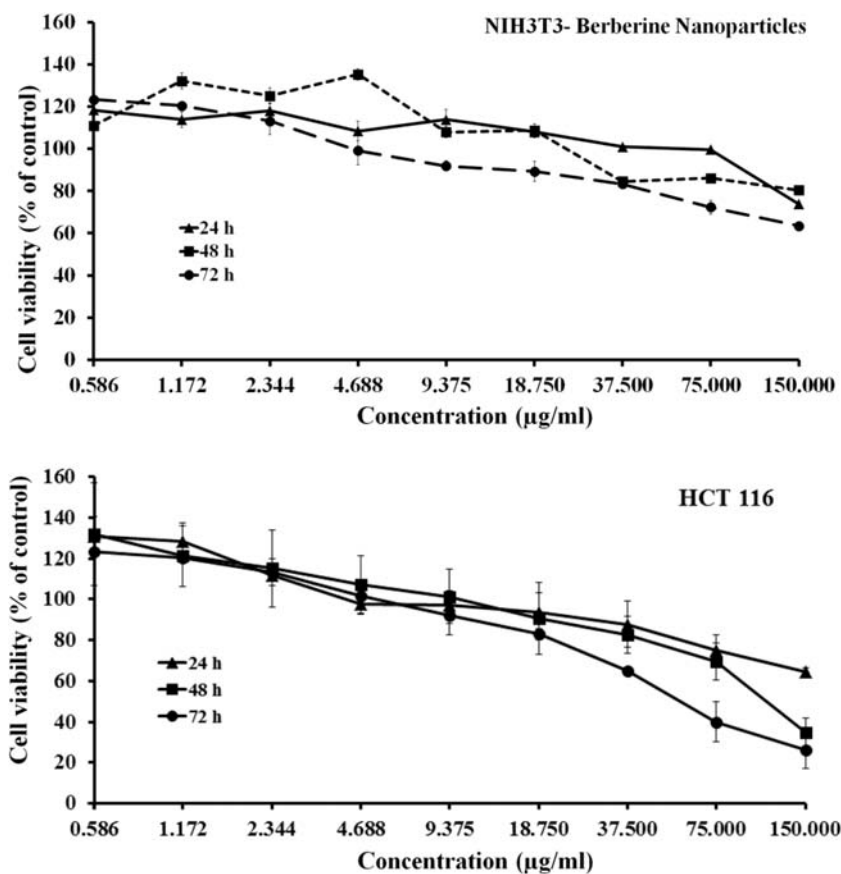

Fig. 9 Colloidal stability study of NPBs

Fig. 10 Cytotoxicity studies of NPs on Fibroblast (b) and HCT116 (c)

in comparison with cancerous cells. This may suggest that nano-formulation may be less toxic against noncancerous cell lines. In addition, BBR caused the growth inhibition of HCT116 and NIH3T3 cells with IC_{50} values of 70.773 and 72.413 μg/mL, respectively.

Cellular uptake of NPBs and BBR

BBR is a fluorescent molecule, which its uptake in the cells can be studied by flow cytometry. Cellular uptake of NPBs and BBR were assessed in HCT116 cells (Fig. 11). Data interpretation demonstrated that the cellular uptake of NPBs was higher than BBR, at both concentrations. The cellular uptake of BBR was 50.3% in comparison with the control, while NPBs showed a considerable increase in cellular uptake to HCT116 cells as 82.9% and 95.0% compared with untreated cells, representing about 2-fold increase when compare with BBR [50].

Discussion

The aim of this study was to develop a cheap, rapid and reliable method to produce drug-loaded NPs in a large scale and with uniformity in size and shape. Accordingly, we used a simplest and cost-effective method known as CES to fabricate NPBs, which were coated with PLA. CES produced NPBs with the least waste of active pharmaceutical ingredients and high DL content and efficacy. In the CES process, the morphology and size of particles are affected by polymer concentration, applied voltage, and the flow rate of solutions. ES or liquid atomization occurs when electrostatic forces overcome the surface tension of a droplet. At this time, the Taylor cone-jet is formed at the tip of the needle. In this research, NPBs were prepared using the CES process and the concentration of PLA, applied voltage and the flow rate of a polymeric solution were discussed. Then, the optimized NPs were characterized and their ability for drug delivery treatment was investigated. Three types of parameters including ambient conditions, process (instrumental), and the solution may affect the ES process. Most of the ambient variables like temperature and humidity and also some instrumental variables like nozzle diameter [[51] were ignored in this study due to the stability of the ambiance and their less impact on the desired output. The ratio of 2:1 (Chloroform:DMF) was chosen as the best solvent for PLA. The R^2 values of the model for size and PSD indicated that the models could be successfully applied to predict size and PSD in the experimental range. The lack of fit of size and PSD was also insignificant, meaning that both models could be utilized for the prediction. According to the graphical plot

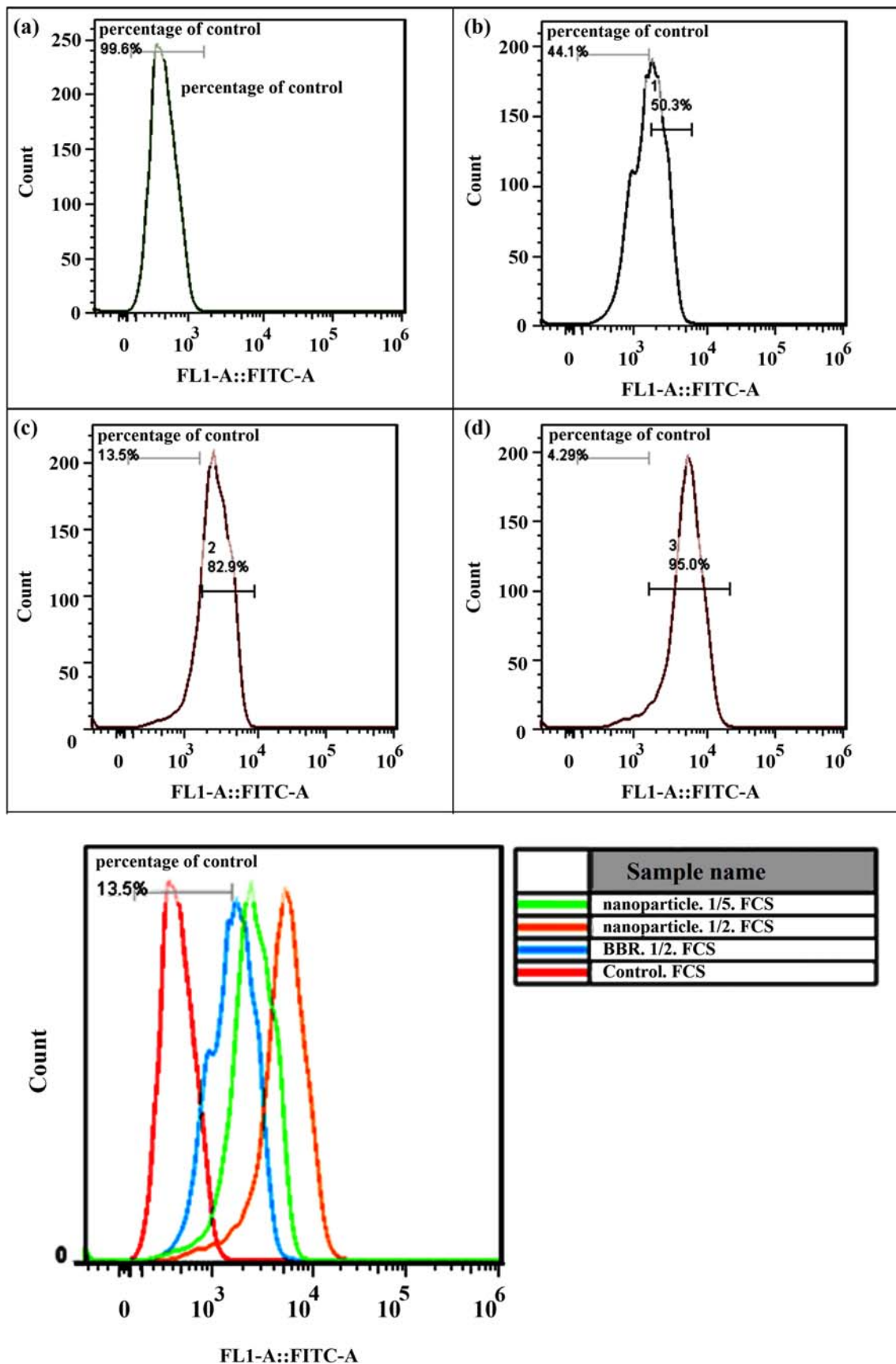**Fig. 11** Cellular uptake of NPBs and BBRin control (**a**), BBR (at 1/2 concentration of its $IC_{50} = 70.773$ μg/mL) (**b**), NPBs (at 1/5 concentration of its $IC_{50} = 56.825$ μg/mL) (**c**), and NPBs (at 1/2 concentration of its $IC_{50} = 56.825$ μg/mL)

Fig. 3a, a highly concentrated solution has high density and high viscosity, which leads to forming a large droplet at the nozzle tip and difficulty of the droplet breakup and consequently, to generating bigger particles. In addition, it is obvious that by decreasing the flow rate from 2 to 1 mL/h, smaller particles have resulted. This result can be explained by the Jaworek and Sobczyke equation, which is based on scaling laws and can justify the trend (**Eq. 9**) [52].

$$d = \alpha \frac{Q^{a_Q} \varepsilon_0^{a_\varepsilon} \rho_l^{a_\rho}}{\sigma_l^{a_\sigma} \gamma_l^{a_\gamma}} \tag{9}$$

d: droplet diameter, Q:volume flow rate, ε_0:permittivity of free space, ρ_1: liquid density, σ_1:liquid surface tension, γ_1:liquid bulk conductivity, and α: a coefficient depending on liquid permittivity.

Figure 3b illustrates the effect of voltage on the final particle size of the NPBs. In fact, by increasing the voltage a decrease in particle size was observable. DMF was added to chloroform to increase the conductivity of the solution, and the Taylor cone was stabilized well. As a result of this stability, charge density on the surface of the Taylor cone was intensified, which led to a facilitated break-up [53] and produced smaller particles. Additionally, **Eq. 10** can prove our claim about the relationship between voltage and particle size [54]. By the equation, an increase in the applied voltage decreased the droplet volume and consequently the size of the NPBs.

$$R_d = \sqrt[3]{\frac{3}{2\rho_l g} \left[r_0 \gamma - 2\varepsilon_0 \left(\frac{V^2}{\ln\left(\frac{4H}{r_0}\right)} \right) \right]} \tag{10}$$

where R_d is the droplet radius (m), γ is the liquid surface tension (N/m), ρ_l is the liquid density (kg/m^3), H is the distance between the tip of the nozzle and the collecting plate (m), r_0 is the radius of the nozzle (m), g is the gravitational acceleration (m/s^2), ε_0 is the permittivity of vacuum and V is the applied voltage (kV).

According to the graphical plot Fig. 4a, an increase in the concentration increased the viscosity of the solution, leading to a conductivity drop [55]. Therefore, a higher voltage was required to combat surface tension and result in a stable cone-jet. Additionally, by increasing the solution flow rate, an increase in PSD was observable. Although some previous studies reported a contrasting result [56], the present research showed a decrease in PSD at low flow rates, which is probably due to the flow regime (laminar flow) and allows the electric field to exert a stronger force on the Taylor cone to stabilize the jet. Three different spray modes may occur during electrospray: single cone-jet, multiple cone-jet, and dripping mode. Droplet size distribution can be influenced by jet type at the tip of the needle. Single cone-jet can produce

monodispersed NPs using the ES method [57]. Figure 4b illustrates the indirect relationship between the applied voltage and PSD. To justify the trend, it should be noted that in a constant concentration, increasing the voltage will increase charge density on the surface of the Taylor cone. Therefore, as a result of charge accumulation, a better break-up will lead to more stability in the cone-jet.

To evaluate the suggested model, the experiments were conducted in optimum condition and the results of SEM images were compared with software results. The obtained suitable precision showed a good agreement between the experimental result and the predicted model, which can be able to predict optimum conditions. The absence of any new functional groups in the FT-IR spectrum of the final nanoparticles indicated that no covalently reaction occurred between PLA and BBR during the CES process. A comparison between synthesized NPBs and physically blended BBR/ PLA demonstrates that all the characteristic peaks of PLA and drug are still present in the physically blended sample but at higher temperatures. This phenomenon can be due to the preservation of the crystalline structure of BBR and PLA. On the other hand, the crystallinity of the NPBs has decreased dramatically which can be justified that by loading and penetrating BBR molecules between PLA chains, the crystallinity of the polymer and BBR is almost gone. Since both BBR and PLA were hydrophobic and BBR was located in the core of the polymer with a high molecular weight, the drug was loaded with high efficiency and acceptable EE and DL. Due to the entrapment of BBR molecules in a polymeric sheath, the BBR release rate from the NPBs was significantly slower than free BBR. In pH 5.8, the drug showed higher solubility, which is due to the interaction between BBR and phosphate salt in lower pHs. Consequently, a more soluble complex was formed [58]. Accordingly, the interaction between PLA chains and drug molecules became weaker, leading to an increase in the release rate of BBR. In the modeling study, the burst release section of the BBR-loaded PLA in pH of 7.4 fitted with Korsmeyer-Peppas modeling. The fast release of the drug could be due to the adsorbed portion of BBR molecules on the surface of the NPs. Moreover, the sustained section of the release profile followed zero-order modeling. At a pH of 5.8, both sections of the burst release and sustained release followed the zero-order modeling. At the first part of the release profile, diffusion was considered as the main release variable, and by water penetration, BBR located on the surface of the NPBs could be released. However, in the sustained release section, the release profile was more controlled like pH of 7.4 and erosion of the NPs may responsible for this behavior. The results revealed that the BBR release was meaningfully influenced by pH values.

Our results indicated that the cytotoxic effect of NPBs (IC_{50} = 56.825 μg/mL) toward cancer cells enhanced in comparison with its free form (IC_{50} = 70.773 μg/mL), indicating that BBR nano-formulation was more toxic and effective to cancer cells than BBR alone. NPBs appeared to have considerable selective toxicity on cancerous cells compared with noncancerous fibroblast cells, which is an important feature of the sample. In vitro and in vivo antitumor efficacy of BBR -nanostructure systems have been confirmed in many studies [45]. For instance, a BBR hydrochloride-loaded solid lipid nanoparticle system inhibited cell proliferation in MCF-7, HepG 2, and A549 cancer cells, although a higher inhibition rate was recorded in MCF-7 cells [59]. MTT assay showed that a BBR-loaded nanostructured lipid carrier inhibited the proliferation of hepatocarcinoma H22 cells with an IC_{50} value of 6.3 μg/mL. On the other hand, co-treatment of BBR and nano-curcumin significantly inhibited the growth of MCF-7 breast cancer cell line with an IC_{50} value of 61.5178 ± 13.58 mg/ml [60]. The flow cytometric analysis indicated that the fluorescence of NPBs taken up by HCT116 colon carcinoma cells was approximately 2-fold higher than BBR, indicating that nanotization could enhance the drug bioavailability.

Conclusions

A new approach was developed in this study to prepare NPBs using the CES process for improving DL and controlled BBR release. Effective variables on size and PSD such as feeding rate, concentration of polymeric solution and applied voltage were studied using the Box-Behnken design. The results revealed that smallest size and PSD values could be obtained in higher voltage and lowest feeding rate in average polymer concentration. Based on the best obtained data, NPBs were prepared and NPBs particles with the mean size of 265 nm and PSD of 43 nm were obtained by SEM images. The entrapment efficacy and BBR loading content of these NPBs were 81% and 7.5%, respectively. The rate of BBR release from NPBs in pH of 5.8 was more than that in physiological pH and had two different release profiles. In the first 12 h, burst release with zero order was observed and after that, sustained release with zero order was detected. NPBs significantly enhanced the cytotoxicity of BBR in comparison with pure BBR, meaning that NPBs were more able to penetrate into cancer cells. We believe that these NPBs may have further potential in cancer drug delivery systems.

Compliance with ethical standards

Conflict of interest The authors declare that they have no conflict of interest.

References

1. Momtaz S, Lall N, Hussein A, Ostad SN, Abdollahi M. Investigation of the possible biological activities of a poisonous south African plant; Hyaenanche globosa (Euphorbiaceae). Pharmacogn Mag. 2010;6(21):34.

2. Rabbani GH, Butler T, Knight J, Sanyal SC, Alam K. Randomized controlled trial of berberine sulfate therapy for diarrhea due to enterotoxigenic Escherichia coli and Vibrio cholerae. J Infect Dis. 1987;155(5):979–84.

3. Jiang H, Wang X, Huang L, Luo Z, Su T, Ding K, et al. Benzenediol-berberine hybrids: multifunctional agents for Alzheimer's disease. Bioorg Med Chem. 2011;19(23):7228–35.

4. Iwasa K, Kim HS, Wataya Y, Lee DU. Antimalarial activity and structure-activity relationships of protoberberine alkaloids. Eur J Med Chem. 1998;13:65–9.

5. Park KD, Lee JH, Kim SH, Kang TH, Moon JS, Kim SU. Synthesis of 13-(substituted benzyl) berberine and berberrubine derivatives as antifungal agents. Bioorg Med Chem. 2006;16(15):3913–6.

6. Singh IP, Mahajan S. Berberine and its derivatives: a patent review (2009 - 2012). Expert Opin Ther Pat. 2013;23(2):215–31.

7. Vennerstrom JL, Lovelace JK, Waits VB, Hanson WL, Klayman DL. Berberine derivatives as antileishmanial drugs. Antimicrob Agents Chemother. 1990;34(5):918–21.

8. Lo CY, Hsu LC, Chen MS, Lin YJ, Chen LG, Kuo CD, et al. Synthesis and anticancer activity of a novel series of 9-O-substituted berberine derivatives: a lipophilic substitute role. Bioorg Med Chem. 2013;23(1):305–9.

9. Yu F, Ao M, Zheng X, Li N, Xia J, Li Y, et al. PEG-lipid-PLGA hybrid nanoparticles loaded with berberine-phospholipid complex to facilitate the oral delivery efficiency. Drug Deliv. 2017;24(1):825–33.

10. Iqbal J, Ejaz SA, Khan I, Ausekle E, Miliutina M, Langer P. Exploration of quinolone and quinoline derivatives as potential anticancer agents. DARU J Pharm Sci. 2019:1–14.

11. Ahmadi Tehrani A, Omranpoor MM, Vatanara A, Seyedabadi M, Ramezani V. Formation of nanosuspensions in bottom-up approach: theories and optimization. DARU J Pharm Sci. 2019;27(1):451–73.

12. Pund S, Borade G, Rasve G. Improvement of anti-inflammatory and anti-angiogenic activity of berberine by novel rapid dissolving nanoemulsifying technique. Phytomedicine. 2014;21(3):307–14.

13. Tan W, Li Y, Chen M, Wang Y. Berberine hydrochloride: anticancer activity and nanoparticulate delivery system. Int J Nanomedicine. 2011;6:1773–7.

14. Sahibzada MUK, Sadiq A, Faidah HS, Khurram M, Amin MU, Haseeb A, et al. Berberine nanoparticles with enhanced in vitro bioavailability: characterization and antimicrobial activity. Drug Des Devel Ther. 2018;12:303.

15. Wang Y, Wen B, Yu H, Ding D, Zhang J, Zhang Y, et al. Berberine hydrochloride-loaded chitosan nanoparticles effectively targets and suppresses human nasopharyngeal carcinoma. J Biomed Nanotechnol. 2018;14(8):1486–95.

16. Yi C, Zhong H, Tong S, Cao X, Firempong CK, Liu H, et al. Enhanced oral bioavailability of a sterol-loaded microemulsion formulation of Flammulina velutipes, a potential antitumor drug. Int J Nanomedicine. 2012;7:5067.

17. Zhu Y, Peng W, Zhang J, Wang M, Firempong CK, Feng C, et al. Enhanced oral bioavailability of capsaicin in mixed polymeric micelles: preparation, in vitro and in vivo evaluation. J Funct Foods. 2014;8:358–66.

18. Zhu Y, Wang M, Zhang Y, Zeng J, Omari-Siaw E, Yu J, et al. In vitro release and bioavailability of silybin from micelle-templated porous calcium phosphate microparticles. AAPS PharmSciTech. 2016;17(5):1232–9.

19. Taghipour YD, Bahramsoltani R, Marques AM, Naseri R, Rahimi R, Haratipour P, et al. A systematic review of nano formulation of natural products for the treatment of inflammatory bowel disease: drug delivery and pharmacological targets. DARU J Pharm Sci. 2018;1.

20. Koupaei SM, Gabris M, Hadi BJ, Baradaran R, Aziz M, Karim K, et al. Adsorption and in vitro release study of curcumin form polyethyleneglycol functionalized multi walled carbon nanotube: kinetic and isotherm study. DARU J Pharm Sci. 2019;27(1):9–20.

21. Hasani M, Sani NA, Khodabakhshi B, Arabi MS, Mohammadi S, Yazdani Y. Encapsulation of Leflunomide (LFD) in a novel niosomal formulation facilitated its delivery to THP-1 monocytic cells and enhanced aryl hydrocarbon receptor (AhR) nuclear translocation and activation. DARU J Pharm Sci. 2019:1–10.

22. Horter D, Dressman JB. Influence of physicochemical properties on dissolution of drugs in the gastrointestinal tract. Adv Drug Deliv Rev. 2001;46(1–3):75–87.

23. Salarpour S, Forootanfar H, Pournamdari M, Ahmadi-Zeidabadi M, Esmaeeli M, Pardakhty A. Paclitaxel incorporated exosomes derived from glioblastoma cells: comparative study of two loading techniques. DARU J Pharm Sci. 2019:1–7.

24. Kumari P, Luqman S, Meena A. Application of the combinatorial approaches of medicinal and aromatic plants with nanotechnology and its impacts on healthcare. DARU J Pharm Sci. 2019:1–15.

25. Al Samad A, Bakkour Y, Fanny C, El Omar F, Coudane J, Nottelet BJPC. From nanospheres to micelles: simple control of PCL-g-PEG copolymers' amphiphilicity through thiol–yne photografting. Polym Chem. 2015;6(28):5093–102.

26. Chopra D, Ray L, Dwivedi A, Tiwari SK, Singh J, Singh KP, et al. Photoprotective efficiency of PLGA-curcumin nanoparticles versus curcumin through the involvement of ERK/AKT pathway under ambient UV-R exposure in HaCaT cell line. Biomaterials. 2016;84:25–41.

27. Zhai SY, Ma YH, Chen YY, Li D, Cao J, Liu YJ, et al. Synthesis of an amphiphilic block copolymer containing zwitterionic sulfobetaine as a novelpH-sensitive drug carrier. Polym Chem. 2014;5:1285–97.

28. Zhao X, Chen S, Lin Z, Du C. Reactive electrospinning of composite nanofibers of carboxymethyl chitosan cross-linked by alginate dialdehyde with the aid of polyethylene oxide. Carbohydr Polym. 2016;148:98–106.

29. Yang JM, Yang JH, Tsou SC, Ding CH, Hsu CC, Yang KC, et al. Cell proliferation on PVA/sodium alginate and PVA/poly (γ-glutamic acid) electrospun fiber. Mater Sci Eng C Mater Biol Appl. 2016;66:170–7.

30. Gómez-Mascaraque LG, Sanchez G, López-Rubio A. Impact of molecular weight on the formation of electrosprayed chitosan microcapsules as delivery vehicles for bioactive compounds. Carbohydr Polym. 2016;150:121–30.

31. Yang YY, Chung TS, Ng NP. Morphology, drug distribution, and in vitro release profiles of biodegradable polymeric microspheres containing protein fabricated by double-emulsion solvent extraction/evaporation method. Biomaterials. 2001;22(3):231–41.

32. Yang Y-Y, Wan J-P, Chung T-S, Pallathadka PK, Ng S, Heller J. POE–PEG–POE triblock copolymeric microspheres containing protein: I. Preparation and characterization J Control Release. 2001;75(1–2):115–28.

33. Cao L, Luo J, Tu K, Wang L-Q, Jiang HJC, Biointerfaces SB. Generation of nano-sized core–shell particles using a coaxial tri-capillary electrospray-template removal method. Colloids Surf B: Biointerfaces. 2014;115:212–8.

34. Ito K, Saito A, Fujie T, Nishiwaki K, Miyazaki H, Kinoshita M, et al. Sustainable antimicrobial effect of silver sulfadiazine-loaded nanosheets on infection in a mouse model of partial-thickness burn injury. Acta Biomater. 2015;24:87–95.

35. Wu X, Ma Y, Zhang G, Chu Y, Du J, Zhang Y, et al. Thermally stable, biocompatible, and flexible organic field-effect transistors and their application in temperature sensing arrays for artificial skin. Adv Mater. 2015;25(14):2138–46.

36. Shao W, He J, Han Q, Sang F, Wang Q, Chen L, et al. A biomimetic multilayer nanofiber fabric fabricated by electrospinning and textile technology from polylactic acid and tussah silk fibroin as a scaffold for bone tissue engineering. Mater Sci Eng C Mater Biol Appl. 2016;67:599–610.

37. Gomez-Estaca J, Balaguer M, Gavara R, Hernandez-Munoz P. Formation of zein nanoparticles by electrohydrodynamic atomization: effect of the main processing variables and suitability for encapsulating the food coloring and active ingredient curcumin. Food Hydrocoll. 2012;28(1):82–91.

38. Quintanilla-Carvajal MX, Camacho-Díaz BH, Meraz-Torres LS, Chanona-Pérez JJ, Alamilla-Beltrán L, Jiménez-Aparicio A, et al. Nanoencapsulation: a new trend in food engineering processing. Food Eng Rev. 2010;2(1):39–50.

39. Barrero A, Ganan-Calvo A, Davila J, Palacio A, Gomez-Gonzalez EJPRE. Low and high Reynolds number flows inside Taylor cones. Phys Rev E. 1998;58(6):7309.

40. Gañán-Calvo AM. The surface charge in electrospraying: its nature and its universal scaling laws. J Aerosol Sci. 1999;30(7):863–72.

41. Lopez-Herrera J, Barrero A, Lopez A, Loscertales I, Marquez M. Coaxial jets generated from electrified Taylor cones. Scaling laws J Aerosol Sci. 2003;34(5):535–52.

42. Zhang L, Huang J, Si T, Xu RX. Coaxial electrospray of microparticles and nanoparticles for biomedical applications. Expert Rev Med Devices. 2012;9(6):595–612.

43. Chakraborty S, Liao I-C, Adler A, Leong KW. Electrohydrodynamics: a facile technique to fabricate drug delivery systems. Adv Drug Deliv Rev. 2009;61(12):1043–54.

44. Faghihi H, Najafabadi AR, Vatanara A. Optimization and characterization of spray-dried IgG formulations: a design of experiment approach. DARU J Pharm Sci. 2017;25(1):22.

45. Mai Z, Chen J, He T, Hu Y, Dong X, Zhang H, et al. Electrospray biodegradable microcapsules loaded with curcumin for drug delivery systems with high bioactivity. RSC Adv. 2017;7(3):1724–34.

46. Rezaei G, Daghighi SM, Raoufi M, Esfandyari-Manesh M, Rahimifard M, Mobarakeh VI, et al. Synthetic and biological identities of polymeric nanoparticles influencing the cellular delivery: an immunological link. J Colloid Interface Sci. 2019;556:476–91.

47. Hartman R, Brunner D, Camelot D, Marijnissen J, Scarlett B. Jet break-up in electrohydrodynamic atomization in the cone-jet mode. J Aerosol Sci. 2000;31(1):65–95.

48. Zhou H-Y, Cao P-P, Zhao J, Wang Z-Y, Li J-B, Zhang F-L. Release behavior and kinetic evaluation of berberine hydrochloride from ethyl cellulose/chitosan microspheres. Front Mater Sci. 2014;8(4):373–82.

49. Khoee S, Yousefalizadeh G, Kavand A. Preparation of dual-targeted redox-responsive nanogels based on pegylated sorbitan for targeted and antitumor drug delivery. Eur Polym J. 2017;95:448–61.

50. Serafim TL, Oliveira PJ, Sardao VA, Perkins E, Parke D, Holy J. Different concentrations of berberine result in distinct cellular localization patterns and cell cycle effects in a melanoma cell line. Cancer Chemother Pharmacol. 2008;61(6):1007–18.

51. Beidokhti HRN, Ghaffarzadegan R, Mirzakhanlouei S, Ghazizadeh L. Dorkoosh. Preparation, characterization, and optimization of folic acid-chitosan-methotrexate core-shell nanoparticles by box-behnken design for tumor-targeted drug delivery. AAPS PharmSciTech. 2017;18(1):115–29.

52. Jaworek A, Sobczyk AT. Electrospraying route to nanotechnology: An overview 2008;66(3–4):197–219.

53. Esmaili Z, Bayrami S, Dorkoosh FA, Akbari Javar H, Seyedjafari E, Zargarian SS, et al. Development and characterization of

electrosprayed nanoparticles for encapsulation of Curcumin. J Biomed Mater Res A. 2018;106(1):285–92.

54. Rezvanpour A, Attia AB, Wang C-HJI. Enhancement of particle collection efficiency in electrohydrodynamic atomization process for pharmaceutical particle fabrication. Ind Eng Chem Res. 2010;49(24):12620–31.

55. Enayati M, Ahmad Z, Stride E, Edirisinghe M. Size mapping of electric field-assisted production of polycaprolactone particles. J R Soc Interface. 2010;7(4):393–402.

56. Ijsebaert JC, Geerse KB, Marijnissen JC, Lammers J-WJ, Zanen P. Electro-hydrodynamic atomization of drug solutions for inhalation purposes. J Appl Physiol. 2001;91(6):2735–41.

57. Karimi Zarchi AA, Abbasi S, Faramarzi MA, Gilani K, Ghazi-Khansari M, Amani A. Development and optimization of N-Acetylcysteine-loaded poly (lactic-co-glycolic acid) nanoparticles by electrospray. Int J Biol Macromol. 2015;72:764–70.

58. Battu SK, Repka MA, Maddineni S, Chittiboyina AG, Avery MA, Majumdar S. Physicochemical characterization of berberine chloride: a perspective in the development of a solution dosage form for oral delivery. AAPS PharmSciTech. 2010;11(3):1466–75.

59. Wang L, Li H, Wang S, Liu R, Wu Z, Wang C, et al. Enhancing the antitumor activity of Berberine hydrochloride by solid lipid nanoparticle encapsulation. AAPS PharmSciTech. 2014;15(4):834–44.

60. ZiaSarabi P, Hesari A, Bagheri M, Baazm M, Ghasemi F. Evaluation of cytotoxicity effects of combination Nano-Curcumin and berberine in breast cancer cell line. IJT. 2018;12(4):47–50.